

## LETTERS

# River plumes as a source of large-amplitude internal waves in the coastal ocean

Jonathan D. Nash<sup>1</sup> & James N. Moum<sup>1</sup>

Satellite images have long revealed the surface expression of large amplitude internal waves that propagate along density interfaces beneath the sea surface<sup>1–3</sup>. Internal waves are typically the most energetic high-frequency events in the coastal ocean<sup>4–6</sup>, displacing water parcels by up to 100 m and generating strong currents and turbulence<sup>7</sup> that mix nutrients into near-surface waters for biological utilization. While internal waves are known to be generated by tidal currents over ocean-bottom topography<sup>8–13</sup>, they have also been observed frequently in the absence of any apparent tide-topography interactions<sup>1,7,14</sup>. Here we present repeated measurements of velocity, density and acoustic backscatter across the Columbia River plume front. These show how internal waves can be generated from a river plume that flows as a gravity current into the coastal ocean. We find that the convergence of horizontal velocities at the plume front causes frontal growth and subsequent displacement downward of near-surface waters. Individual freely propagating waves are released from the river plume front when the front's propagation speed decreases below the wave speed in the water ahead of it. This mechanism generates internal waves of similar amplitude and steepness as internal waves from tide-topography interactions observed elsewhere<sup>11</sup>, and is therefore important to the understanding of coastal ocean mixing.

It is generally assumed that internal waves radiate from locations where tidal currents flow over topographic features such as shelf-breaks<sup>10</sup>, banks<sup>11</sup> and sills<sup>12,13</sup>. In the last case, waves formed downstream of a sill are trapped to the topography when their wavespeed  $c$  equals that of the opposing tidal flow  $u$ . They are released and propagate upstream as free waves when  $u$  slackens below  $c$  (refs 8, 9, 15). The Froude number  $F = u/c \leq 1$  sets the criterion for free wave propagation.

In the atmosphere, gravity currents<sup>16</sup> are well-known to excite large-amplitude waves. Perhaps the most famous is the 'Morning Glory', a series of ~500-m amplitude undulations over the Gulf of Carpentaria off northern Australia<sup>17,18</sup>. Wave generation from gravity currents has also been observed in thunderstorm outflows<sup>19</sup> and mountain slope drainage winds<sup>20</sup>. However, the large scales of atmospheric flows make it difficult to obtain the detailed measurements necessary to show the process by which freely propagating waves emerge from a gravity current. Although laboratory experiments<sup>21,22</sup> have helped to show this evolution, these experiments were limited to small, sub-geophysical scales. Neither atmospheric nor laboratory observations have clearly defined the criterion for wave release.

Rivers issue into the coastal ocean as tidally modulated pulses of fresh water that form positively buoyant gravity currents<sup>23</sup>. The evolving properties of these gravity currents are determined by the initial momentum at the river's mouth, by interactions with coastal currents and winds, and by the Earth's rotation, which tends to turn the current to the right in the Northern Hemisphere. These factors all

affect the location, propagation speed and sharpness of the gravity current front.

Satellite images capture single snapshots of waves radiating from the mouth of the Columbia River (Fig. 1; refs 1, 2). However, they provide no information on the waves' internal structure. Nor do they show the sequence of events leading to their generation, since these images are acquired infrequently (<1 per day). Our recent *in situ* observations across a front at the northern edge of the tidally pulsing Columbia River plume provide the necessary sequencing to clearly define the condition for the formation of large-amplitude internal waves from a gravity current. By analogy to topographic release of waves from a sill, this condition is described in terms of a Froude number.

Satellite sea surface temperature (SST) distinguishes the warm, summertime plume from cold, recently upwelled coastal waters (Fig. 2a–c) on 23 July 2004. High tide coincided with the image shown in Fig. 2a. Plume remnants from the previous tidal cycle's discharge appear in the offshore thermal structure. Ebb currents started to flow

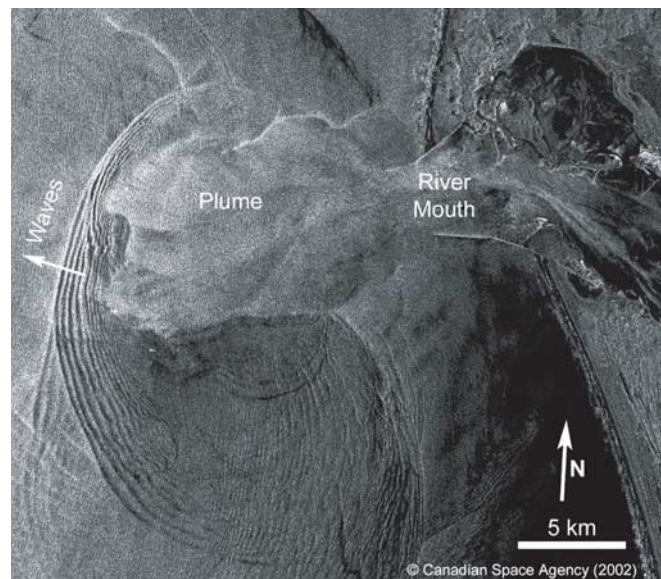


**Figure 1 | Synthetic aperture radar (SAR) image of the Columbia River plume on 9 August 2002.** Image indicates regions of enhanced surface roughness associated with plume-front and internal wave velocity convergences. Similar features appear in images during all summertime months (April–October; see <http://oceanweb.ocean.washington.edu/rise/data.htm> for more Columbia River plume images) and from other regions<sup>1,2</sup>. SAR image courtesy of P. Orton, T. Sanders and D. Jay; image was processed at the Alaska Satellite Facility, and is copyright Canadian Space Agency.

<sup>1</sup>College of Oceanic and Atmospheric Sciences, Oregon State University, 104 COAS Admin Bldg, Oregon State University, Corvallis, Oregon 97331, USA.

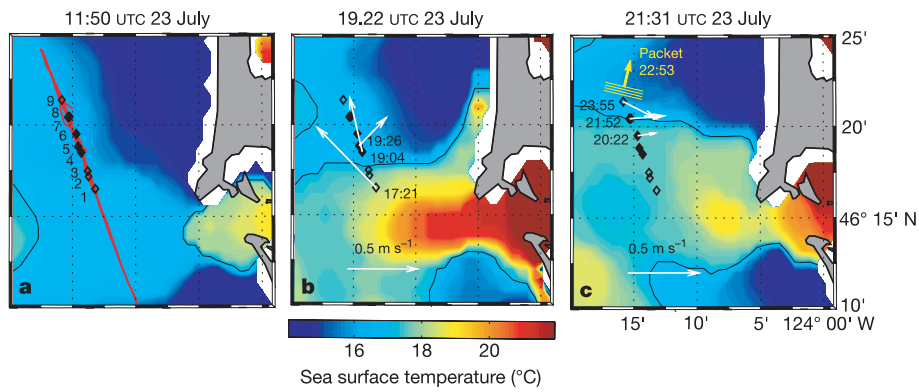


**Figure 2 | Progression of the Columbia River plume from satellite-derived SST images.** Times (23 July 2004 UTC) are 11:50 (a), 19:22 (b) and 21:31 (c). Red line in left panel is ship track. Diamonds show locations where plume front was crossed; filled diamonds correspond to the four crossings presented in Fig. 3. Near-surface fluid velocities behind the plume front  $u_p$  at

selected crossings are indicated in b and c (45-s average over  $0\text{ m} < z < 5\text{ m}$ ); vectors are grouped to correspond to time of SST images. The  $17^\circ\text{C}$  isotherm is contoured and represents the approximate front location. Location of the wave packet at 22:53 as imaged by shipboard X-band radar is shown in c.

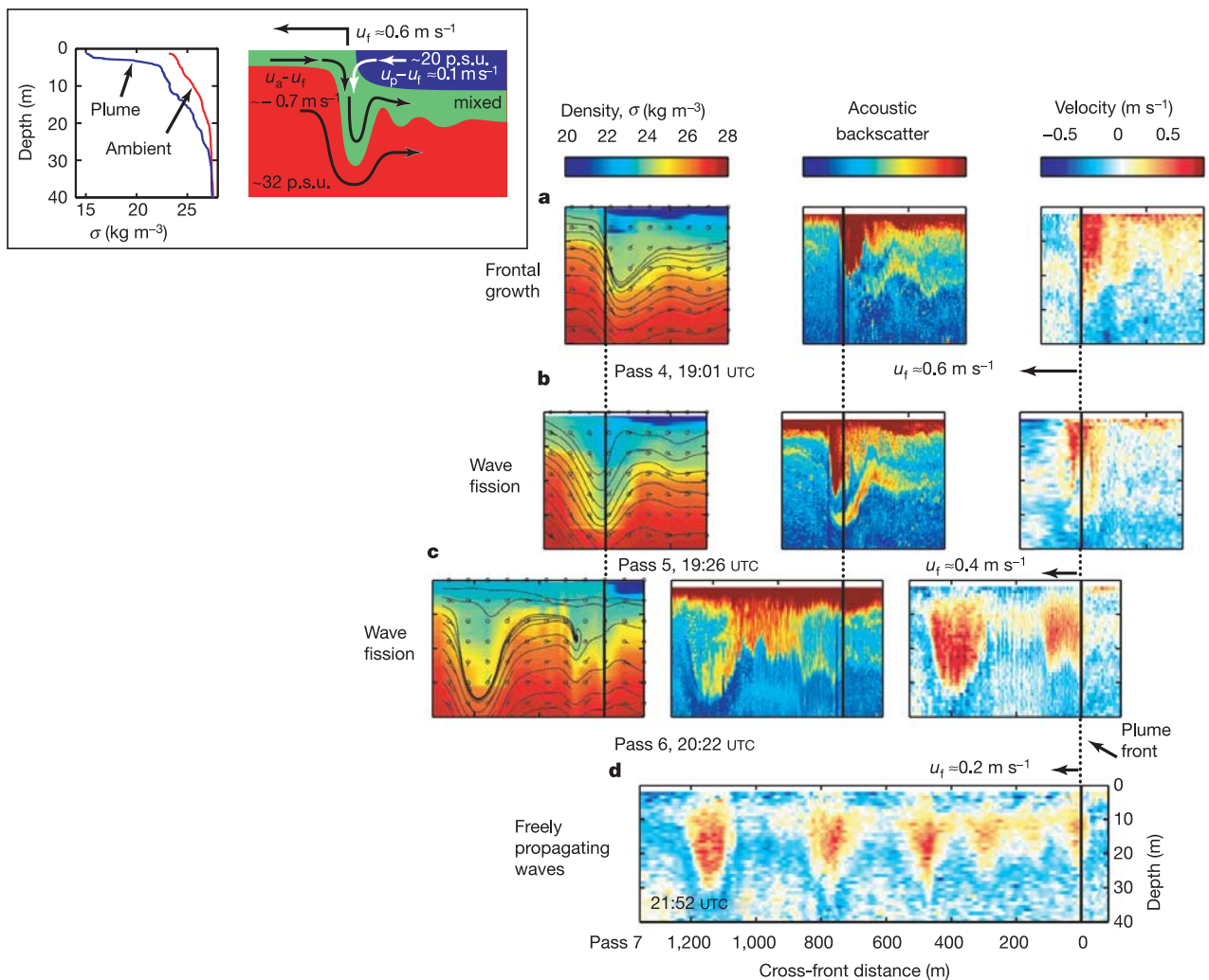


**Figure 3 | Three stages of a wave-generation event.** a, Frontal growth at the plume's leading edge; b, c, wave fission from the plume front; and d, free propagation of a train of large-amplitude internal waves. Shown are density (left), acoustic backscatter (middle) and cross-front component of horizontal velocity (right) in a reference frame aligned with the front (see Methods). Positive distances and velocities are approximately northward; velocities are relative to a stationary reference frame. Panels are shifted to align the plume front (as determined from sea surface salinity); vertical black lines represent the plume front (zero cross-front distance). Only cross-front

velocity is shown for the freely propagating waves in d. Particle streamlines and velocity vectors ( $u, w$ ) in a reference frame moving with the front (translating at speed  $u_f$  as indicated) are contoured over the density plots. A schematic cartoon illustrating frontal growth in a reference frame moving with the plume front (at speed  $u_f$ ) is shown in upper left inset. Velocities of the near-surface fluid behind the plume front ( $u_p$ ) and ambient water ahead of it ( $u_a$ ) are indicated. Also shown for pass 4 (panel a) are vertical profiles of density ahead of (red, ambient) and behind (blue, plume) the front.

shortly thereafter, producing a pulse of fresh and warm water visible in Fig. 2b. At 19:00 UTC, the plume front flowed northward as a gravity current with  $u_f \approx 0.6 \text{ m s}^{-1}$  (Fig. 2b), opposed by weak winds from the north and a southward near-surface current ( $u_a \approx -0.1 \text{ m s}^{-1}$ ) that helped sharpen the front. ( $u_f$  and  $u_a$  represent the cross-front components of the frontal propagation speed and the velocity of ambient fluid ahead of the front.) 1.5 h later, plume-front velocities turned eastward (Fig. 2c). During this transition period, a packet of waves was released.

Cross-front snapshots of velocity, density and acoustic backscatter capture the growth of the plume front, the release of two individual waves, and the free propagation of a train of waves away from the plume front (Fig. 3). In its initial phase, the plume front moved northward at  $\sim 0.6 \text{ m s}^{-1}$  and vertical displacements at the front grew to 20 m during a  $\sim 2$ -h period (Fig. 3a). Twenty-five minutes later (Fig. 3b), the cross-front component of the plume velocity weakened and the isopycnal depression at the plume front (now almost 25 m) separated from it. One hour later (Fig. 3c), this distinct and solitary wave had propagated 400 m ahead of the plume front, and a second wave emerged. Following this, a train of freely propagating internal waves were observed (Fig. 3d). The full generation sequence is summarized as a progression: frontal growth  $\rightarrow$  wave fission  $\rightarrow$  freely propagating waves. The space-time plot (Fig. 4) of front, wave and ship locations illustrates this progression.

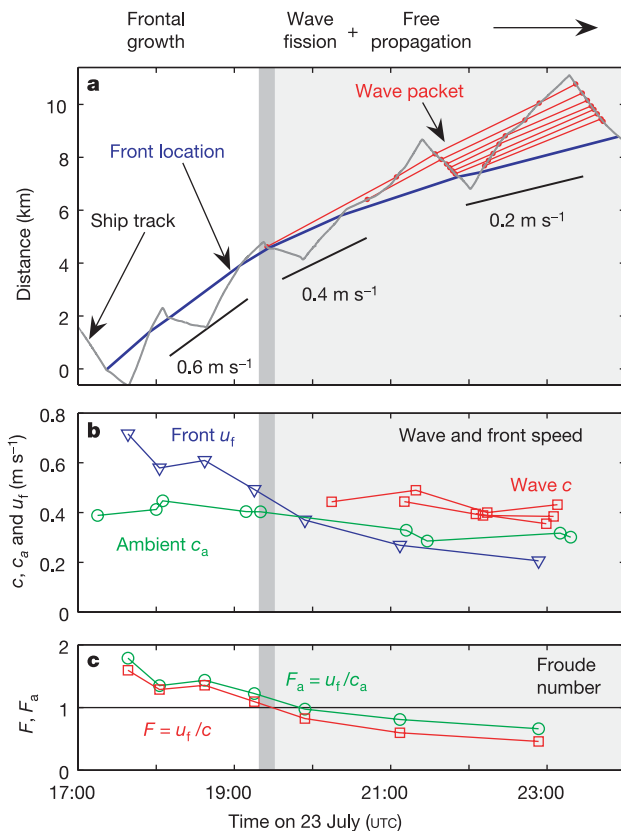


**Figure 4 | Time-evolution of plume front and wave packet.** **a**, Location of ship (grey), plume front (blue) and wavepacket (red) as a function of time. Ordinate is distance from the first frontal crossing along a curved trajectory perpendicular to either plume front or leading wave. **b**, The speed of the plume front ( $u_f$ , blue) as computed from the rate of change of front location. The first-mode linear wavespeed ahead of the plume ( $c_a$ , green) reflects the slowly-changing background density and velocity structure in the ambient ocean; observed wavespeeds computed from first-differences of wave location ( $c$ , red) are higher. Corresponding Froude numbers are shown in **c**;  $F$  was computed using  $c = 0.45 \text{ m s}^{-1}$ . The vertical grey bar represents the first wave fission event (Fig. 3b) and  $F = 1$ ; light shading represents the domain over which fission and free propagation are permitted ( $F < 1$ ).

In analogy to topographic control, the Froude number  $F = u_f/c$  based on the frontal velocity  $u_f$  is a natural parameter governing the flow<sup>22,24,25</sup>. In a reference frame moving with the front,  $F$  represents the ratio of the opposing flow speed required to keep the front stationary ( $u_f$ ), to the internal wavespeed in the medium into which the front advances ( $c$ ).

In a fluid with vertical gradients in both density and velocity, the intrinsic speed of a long, small-amplitude linear wave is determined from the hydrostatic Taylor-Goldstein equation<sup>26</sup>. Intrinsic wave-speeds in the ambient coastal waters ( $c_a \approx 0.4 \text{ m s}^{-1}$ ; Fig. 4b) are roughly half that within the highly stratified brackish plume. Measured wavespeeds in the ambient waters ( $c$ ) are  $\sim 30\%$  greater than  $c_a$  owing to finite amplitude effects<sup>6</sup>. We may thus form two Froude numbers: (1)  $F_a = u_f/c_a$  based on the intrinsic properties of the ambient fluid, and (2)  $F = u_f/c$  based on the measured wavespeed in that medium (Fig. 4b, c).  $F_a$  always exceeds  $F$ .

Initially the front moves at a speed  $u_f$  that exceeds both  $c_a$  and  $c$  ( $F > 1$ ; Fig. 4b). During this phase, horizontal velocity convergence at the plume's edge is intense (Fig. 3a;  $\Delta u \approx 1 \text{ m s}^{-1}$  in  $\Delta x' = 10 \text{ m}$ ) and drives  $>0.3 \text{ m s}^{-1}$  vertical velocities. (See Methods for definition of  $x'$ .) This convergence provides a means of converting the gravity current's kinetic energy to potential energy. Since the frontal velocity exceeds all internal wavespeeds ahead of the front, this potential energy is trapped at the front and cannot radiate ahead of it (Fig. 4a, b). Waves may, however, propagate back towards the plume source<sup>27</sup>, but these were not captured in this study.

As the plume front decelerates,  $F$  decreases below unity (Fig. 4c); wave fission ensues. With the transition of  $F$  from super- ( $F > 1$ ) to subcritical ( $F < 1$ ), the depression that was originally locked to the freshwater front advances into the ambient fluid as a freely propagating wave. In this way, the wave inherits the vertical displacement structure of the front. Because  $c$  increases with amplitude<sup>6</sup>,  $F$  also decreases as frontal vertical displacements grow. It is therefore impossible to predict the precise timing of fission from  $F_a$  alone. Only when frontal amplitudes are sufficiently large does  $c$  exceed  $u_f$ , permitting fission to occur.

Following fission of the first wave (Fig. 3b), sustained convergence at the front continues to displace fluid downward, creating anew the disturbance from which subsequent waves emerge. In Fig. 3b, the wave is  $\sim 50 \text{ m}$  ahead of the freshwater front, moving to 400 m ahead in Fig. 3c, by which time the front has regenerated its vertical displacement to sufficient amplitude for a second wave to release.

Once released, waves propagate freely at  $c \approx 0.40 - 0.45 \text{ m s}^{-1}$  with 20-m amplitude (Fig. 4b). These were tracked more than 5 km from their release location (Fig. 4a). Meanwhile, the increasingly subcritical front forces waves with successively smaller amplitude. This factor, together with reduced convergence, limits frontal growth and restricts the amplitudes of the released waves. By the time of our last crossing, the frontal velocity gradient had been reduced to  $<0.4 \text{ m s}^{-1}$  over 1,000 m. Ultimately, the front loses its velocity signature entirely.

In summary, internal waves generated from the Columbia River plume are of similar amplitude and steepness to those generated over topography elsewhere in the coastal ocean<sup>10</sup>. Although less energetic than some waves which propagate through deep water (for example, through the South China Sea<sup>28</sup>), these plume-generated internal waves are large compared to the local water depth, and have important implications for biology and turbulent mixing.

Wave fission from a decelerating gravity current represents an important mechanism for generation of large-amplitude internal waves in the coastal ocean and explains their existence in the absence of a topographic generation site<sup>2,14</sup>. The Froude number criterion controlling the timing of wave fission is analogous to that of topographic generation; that is, in each case, free propagation occurs when the wavespeed exceeds the background velocity that arrests the disturbance. For topographic control, that velocity is relative to topography<sup>8</sup>; for a gravity current, that velocity is relative to the

propagating front<sup>22</sup>. This mechanism will be realized for any river with discharge velocities exceeding coastal internal wavespeeds.

## METHODS

Density, biological fluorescence and turbulence profiles were obtained from within 2 m of the surface to the bottom using the Chameleon turbulence profiler<sup>23</sup>; its horizontal resolution is limited by the unequal but nominally 100-m spacing between profiles. Our perspective of the structure of the waves and front is augmented with a rapidly sampled echosounder (Biosonics 120 kHz; acoustic scatterers include zooplankton and density microstructure) and acoustic Doppler current profiler (ADCP; RD Instruments 300 kHz), both mounted 1 m beneath the sea surface

Nine transects across the plume front were acquired as part of an interdisciplinary effort to understand river influences in coastal ecosystems (<http://www.ocean.washington.edu/rise/index.htm>). Front and wave locations were determined from Chameleon density and ADCP velocity profiles. Frontal orientation was determined by combining X-band shipboard radar and ADCP velocity. The front was assumed perpendicular to the wave-induced fluid velocities, consistent with available radar images. The distance from the leading wave  $x'$  is  $x' = [\mathbf{x} - \mathbf{x}_w(t)] \cdot \mathbf{n}$ , where  $\mathbf{x}$  is a measurement location,  $\mathbf{x}_w(t)$  is the location of the leading wave at time  $t$  as computed from a linear interpolation of the crossings, and  $\mathbf{n}$  is the unit vector normal to the front (and in the direction of wave propagation). The distance between the leading wave and the plume front (as determined from the surface salinity) is subtracted from  $x'$  to yield the cross-front distance in Fig. 3. This coordinate transformation minimizes spatial Doppler shifting (the tendency for features to look compressed or elongated when measured from a moving platform) at the expense of smearing temporal information (approximately 1 h of data goes into each image). We implicitly assume that changes in the waveform are small over each transect's duration.

Eigenvalues and eigenvectors of the Taylor-Goldstein equation provide the propagation speeds and vertical structure functions for long wavelength, small amplitude, hydrostatic disturbances<sup>26</sup>. These solutions depend only on the density stratification and velocity shear of the background flow, so they are intrinsic to the medium. To predict finite amplitude wavespeeds, higher-order corrections are required, such as that provided through solutions of the Korteweg de Vries (KdV) equation<sup>6</sup>. Solutions to the KdV equation for a 20-m wave in a non-sheared medium suggest an increase of 30–40% in wavespeed over the linear modes (when computed using the Taylor-Goldstein equation in a non-sheared medium). This is in accord with measured wavespeeds, for which a similar ~30% increase is observed as compared to the linear wavespeeds in a sheared medium. Finite amplitude wavespeeds in a sheared medium have not been computed.

Received 10 March; accepted 13 June 2005.

1. Fu, L. L. & Holt, B. *Seasat Views Oceans and Sea Ice with Synthetic-Aperture Radar* (JPL publication 81-120, NASA Jet Propulsion Laboratory, Pasadena, 1982).
2. Jackson, C. & Apel, J. An atlas of internal solitary-like waves and their properties. ([http://www.internalwaveatlas.com/Atlas2\\_index.html](http://www.internalwaveatlas.com/Atlas2_index.html)) 2004.
3. Ray, R. D. & Mitchum, G. T. Surface manifestation of internal tides generated near Hawaii. *Geophys. Res. Lett.* **23**, 2101–2104 (1996).
4. Huthnance, J. M. Internal tides and waves near the continental shelf edge. *Geophys. Astrophys. Fluid Dyn.* **48**, 81–105 (1989).
5. Osborne, A. R. & Burch, T. L. Internal solitons in the Andaman Sea. *Science* **208**, 451–460 (1980).
6. Ostrovsky, L. & Stepanyants, Y. Do internal solitons exist in the ocean? *Rev. Geophys.* **27**, 293–310 (1989).
7. Moun, J. N., Farmer, D. M., Smyth, W. D., Armi, L. & Vagle, S. Structure and

generation of turbulence at interfaces strained by internal solitary waves propagating shoreward over the continental shelf. *J. Phys. Oceanogr.* **33**, 2093–2112 (2003).

8. Maxworthy, T. A note on the internal solitary waves produced by tidal flow over a three-dimensional ridge. *J. Geophys. Res.* **84**, 338–346 (1979).
9. Lamb, K. G. Numerical experiments of internal wave generation by strong tidal flow across a finite amplitude bank edge. *J. Geophys. Res.* **99**, 843–864 (1994).
10. Cherskin, T. K. Generation of internal waves in Massachusetts Bay. *J. Phys. Oceanogr.* **88**, 2649–2661 (1983).
11. Loder, J. W., Brickman, D. & Horne, E. P. W. Detailed structure of currents and hydrography on the northern side of Georges Bank. *J. Geophys. Res.* **97**, 14331–14351 (1992).
12. Farmer, D. M. & Smith, J. D. in *Hydrodynamics of Estuaries and Fjords* (ed. Nihoul, J.) 465–493 (Elsevier, Amsterdam, 1978).
13. Farmer, D. M. & Armi, L. The generation and trapping of solitary waves over topography. *Science* **283**, 188–190 (1999).
14. Stanton, T. P. & Ostrovsky, L. A. Observations of highly nonlinear internal solitons over the continental shelf. *Geophys. Res. Lett.* **25**, 2695–2698 (1998).
15. Sutherland, B. R. Interfacial gravity currents. I. Mixing and entrainment. *Phys. Fluids* **14**, 2244–2254 (2002).
16. Simpson, J. E. *Gravity Currents in the Environment and Laboratory* (Cambridge Univ. Press, Cambridge, UK, 1987).
17. Christie, D. R., Muirhead, K. J. & Clarke, R. H. Solitary waves in the lower atmosphere. *Nature* **293**, 46–49 (1981).
18. Smith, R. K., Crook, N. & Roff, G. The Morning Glory: An extraordinary atmospheric undular bore. *Q. J. R. Meteorol. Soc.* **108**, 937–956 (1982).
19. Doviak, R. J., Chen, S. S. & Christie, D. R. Thunderstorm-generated solitary wave observation compared with theory for nonlinear waves in a sheared atmosphere. *J. Atmos. Sci.* **48**, 87–111 (1991).
20. Rao, M. P., Castracane, P., Casadio, S., Fua, D. & Fiocco, G. Observations of atmospheric solitary waves in the urban boundary layer. *Boundary-Layer Meteorol.* **111**, 85–108 (2004).
21. Rottman, J. W. & Simpson, J. E. The formation of internal bores in the atmosphere: A laboratory model. *Q. J. R. Meteorol. Soc.* **115**, 941–963 (1989).
22. Maxworthy, T., Leilich, J., Simpson, J. E. & Meiburg, E. H. The propagation of a gravity wave into a linearly stratified fluid. *J. Fluid Mech.* **453**, 371–394 (2002).
23. Orton, P. M. & Jay, D. A. Observations at the tidal plume front of a high-volume river outflow. *Geophys. Res. Lett.* **32**, L11605 doi:10.1029/2005GL02237 (2005).
24. Britter, R. E. & Simpson, J. E. Experiments on the dynamics of a gravity current head. *J. Fluid Mech.* **88**, 223–240 (1978).
25. Luketina, D. A. & Imberger, J. Characteristics of a surface buoyant jet. *J. Geophys. Res.* **92**, 5435–5447 (1987).
26. Drazin, P. G. & Reid, W. H. *Hydrodynamic Stability* (Cambridge Univ. Press, Cambridge, 1981).
27. O'Donnell, J. & Garvine, R. W. A time dependant, two layer frontal model of buoyant plume dynamics. *Tellus A* **35**, 73–80 (1983).
28. Duda, T. F. et al. Internal tide and nonlinear internal wave behaviour at the continental slope in the Northern South China Sea. *IEEE J. Ocean. Eng.* **20**, 1105–1130 (2004).
29. Moun, J. N., Gregg, M. C., Lien, R. C. & Carr, M. Comparison of turbulence kinetic energy dissipation rate estimates from two ocean microstructure profilers. *J. Atmos. Ocean. Technol.* **12**, 346–366 (1995).

**Acknowledgements** We thank M. Neeley-Brown, R. Kreth and A. Perlin for their technical expertise. L. Kilcher, T. Kimura, R. Bjorkquist, A. Horner-Devine, T. Chisholm, and the captain and crew of the RV *Pt. Sur* made data collection possible. Satellite imagery was provided by P.T. Strub and P. Orton. Comments were provided by W.D. Smyth, G. Avicola and J. Klymak. This work was funded by the National Science Foundation and the Office of Naval Research.

**Author Information** Reprints and permissions information is available at [npg.nature.com/reprintsandpermissions](http://npg.nature.com/reprintsandpermissions). The authors declare no competing financial interests. Correspondence and requests for materials should be addressed to J.D.N. ([nash@coas.oregonstate.edu](mailto:nash@coas.oregonstate.edu)).